**Jessica Burgner**
e-mail: jessica.burgner@vanderbilt.edu

**Philip J. Swaney**
e-mail: philip.j.swaney@vanderbilt.edu

**Trevor L. Bruns**
e-mail: trevor.l.bruns@vanderbilt.edu

**Marlena S. Clark**
e-mail: marlena.s.clark@vanderbilt.edu

**D. Caleb Rucker**
e-mail: daniel.c.rucker@vanderbilt.edu

Department of Mechanical Engineering,
Vanderbilt University,
2400 Highland Avenue,
Nashville, TN 37212

**E. Clif Burdette**
Acoustic MedSystems Inc.,
208 Burwash Avenue,
Savoy, IL 61874
e-mail: clifb@acousticmed.com

**Robert J. Webster**
Department of Mechanical Engineering,
Vanderbilt University,
2400 Highland Avenue,
Nashville, TN 37212
e-mail: robert.webster@vanderbilt.edu

# An Autoclavable Steerable Cannula Manual Deployment Device: Design and Accuracy Analysis

*Accessing a specific, predefined location identified in medical images is a common interventional task for biopsies and drug or therapy delivery. While conventional surgical needles provide little steerability, concentric tube continuum devices enable steering through curved trajectories. These devices are usually developed as robotic systems. However, manual actuation of concentric tube devices is particularly useful for initial transfer into the clinic since the Food and Drug Administration (FDA) and Institutional Review Board (IRB) approval process of manually operated devices is simple compared to their motorized counterparts. In this paper, we present a manual actuation device for the deployment of steerable cannulas. The design focuses on compactness, modularity, usability, and sterilizability. Further, the kinematic mapping from joint space to Cartesian space is detailed for an example concentric tube device. Assessment of the device's accuracy was performed in free space, as well as in an image-guided surgery setting, using tracked 2D ultrasound.* [DOI: 10.1115/1.4007944]

## 1 Background and Motivation

Percutaneous access to a specific, predefined location is a common surgical task required to perform biopsies and drug or therapy delivery (e.g., thermal ablation). The current surgical instruments of choice for these procedures are needles. Insertion and steering is usually supported by medical imaging, such as ultrasound or fluoroscopy. Mapping the instrument position from a 2D image to an actual 3D position and orientation within the patient is a challenging task for the surgeon. To make matters worse, the steering capabilities of conventional needles are limited, i.e., usually restricted to straight access paths.

Over the last decade, research efforts have led to advanced needle steering approaches that enable for controlled curved insertion paths within tissue [1–5]. These techniques make use of the tissue itself to enable steering through interaction forces. Hence, control of the insertion path requires accurate knowledge of the tissue mechanical properties and boundary conditions [6]. The reliable determination of these parameters *in situ* with high fidelity and incorporation of inhomogeneous tissue properties are open research challenges. Furthermore, these steerable needle approaches cannot be used in air or liquid-filled cavities.

Concentric tube devices, also known as active or steerable cannulas, provide dexterous steering capabilities without relying on tissue interaction forces, while maintaining the compactness of needles [7–9]. These devices are composed of multiple, precurved, superelastic, concentric tubes. Steering is achieved by actuation of the tubes with respect to each other, i.e., translation and axial rotation of each tube. When many tubes are used, robotic actuation is preferred for these devices. However, manual actuation may be desirable for selected medical applications for the following reasons: (1) to acquaint surgeons with this type of device while leaving them still in full control of the procedure, (2) to speed up clinical translation via an easier route through IRB and FDA approval, and (3) when only a small number of tubes is involved and dynamic motion is not required.

Typically, prior concentric tube devices have been designed to work as miniature manipulators in open [10] or liquid filled cavities [11]. In applications where these devices act as steerable needles embedded in soft tissues, it is important to design them to be capable of advancing in such a way that the shaft exactly follows the tip's trajectory through tissue. General combinations of tubes cannot achieve this. Even a concentric tube device as simple as two tubes with circular precurvatures can only achieve this when the precurvatures are perfectly aligned in the same plane, such that there is zero torsion [12]. The only design that has been suggested to date where the shaft will exactly follow the tip as it advances, consists of a straight outer tube and a curved inner tube, which carries a straight, elastic interventional instrument within it [13–16]. Through this specific design, under the assumption of negligible friction, together with a specific deployment sequence (described later in this paper), torsion is avoided everywhere in the device at all times.

In Refs. [13–15], preliminary studies were presented toward thermal tumor ablation using the concentric tube principle to steer

Manuscript received February 3, 2012; final manuscript received September 14, 2012; published online November 21, 2012. Assoc. Editor: James Moore.

  

an ablator to multiple predefined locations within the liver though a single liver capsule entry point. This is desirable to minimize bleeding and trauma to the organ. Tracked 2D ultrasound and elastography were used for image-guidance and monitoring of the ablation process. In this paper, we focus on the mechanical design elements of this large project. We present an archival unification of some results previously presented in preliminary form at conferences, along with new accuracy assessment experiments. These results include the design of an autoclavable steerable cannula deployment device [16] and forward kinematic and inverse kinematic mappings for the steerable cannula (we present a clarified and updated version of the equations originally appearing in Ref. [14], which is a special case of Ref. [17]). In addition to archival unification of these prior results, we have added an experimental assessment of the achievable targeting accuracy in free space and in an ultrasound-guided setting, under the assumption that the tubes are much stiffer than the surrounding media and will not deform as they advance through it.

## 2 Steerable Cannula Deployment Device

The design of our manual actuation device centers around accomplishing several goals:

**Mechanical Criteria:** The device needs to meet the basic criteria for actuating the steerable cannula. Namely, it must nonbackdrivably hold multiple tubes in axial alignment, individually translate each along their common axis, and rotate each tube axially independently of the others.

**Versatility:** The actuation unit should be adaptable and versatile enough to allow the same device to be used in a variety of medical applications. Thus, the tubes should be replaceable and the device able to accommodate a range of tube diameters and lengths.

**Compactness:** The device should be as compact as possible in order to fit seamlessly into the operating room environment, where space is at a premium.

**Usability:** It is also necessary that the apparatus is easy to use for the operator while achieving high precision and reliability.

**Sterilizability:** Since the device is to be used in the operating room and is not intended to be disposable, the device will be most useful if it can be sterilized in a standard autoclave. A typical steam autoclave operates at approximately 120 °C for approximately 15 min. Thus, in order to withstand autoclaving, we designed our actuation unit to contain no oil lubrication and consist exclusively of materials that are rated to at least 150 °C.

**2.1 Concept and Design.** Our manual actuation device prototype, depicted in Fig. 1, actuates a two tube cannula. We note that the design allows straightforward extension to multiple tubes due to a modular carrier design where each holds one tube. The device consists of two carriers that move along a base. The unit allows easy mounting to various positioning/holding devices depending on the application (e.g., passive holding arms attached to the rails of operating tables). All components are made of aluminum unless otherwise specified.

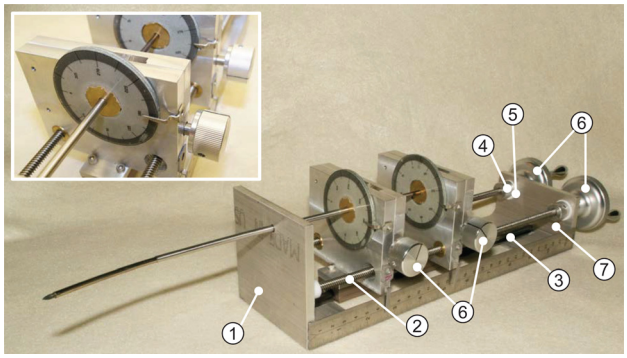


**Fig. 1 Prototype of a manual actuation device for steerable cannulas. Mechanical parts are: (1) front plate, (2) lead screws, (3) linear rail, (4) lead screw stops, (5) PTFE washers, (6) control knobs, and (7) back plate.**

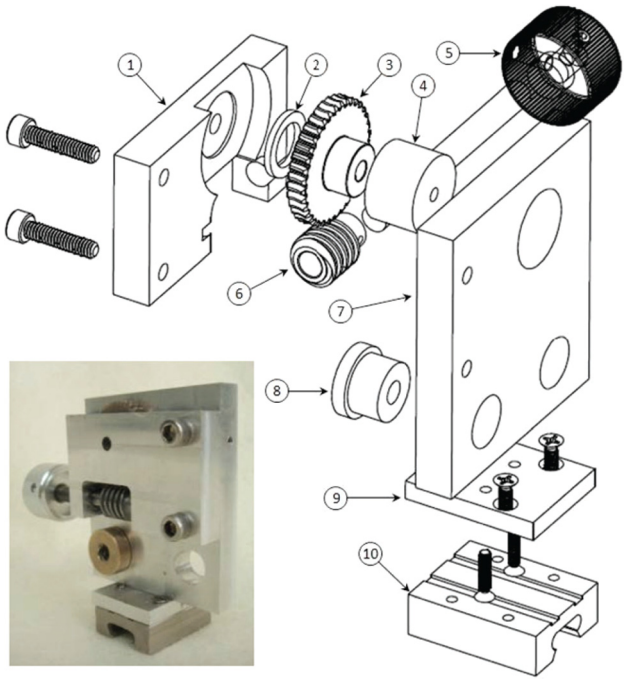


**Fig. 2 Tube carrier mechanism. Exploded view with rotational housing (1), washer (2), worm gear (3), tube adapter (4), control knob (5), worm (6), main plate (7), lead screw nut (8), mounting plate (9), and linear guide block (10).**

*2.1.1 Carriers.* The primary components of the device are the individual tube carriers. An exploded view of a carrier is shown in Fig. 2. Each carrier is responsible for actuating a single tube. The tubes are rigidly held by a tube adapter (Fig. 2, part 4) to which the tube is affixed with three set screws. Furthermore, for clinical use, we foresee the tubes and the tube adapters being disposable. The tube adapter fits over a brass worm gear (Fig. 2, part 3) and is held in place by a set screw (Fig. 3, part 3). As the control knob (Fig. 2, part 5) is turned, it rotates a steel worm (Fig. 2, part 6) in order to angularly position the tube about its axis. There is a 36:1 gear ratio between the worm and worm gear. Thus, one full turn of the control knob will rotate the tube by 10 deg. A brass washer (Fig. 2, part 2) reduces friction between the worm gear and housing (Fig. 2, part 1). The housing is secured to the main plate (Fig. 2, part 7) by two screws. These are tightened to hold the worm gear securely, while still allowing rotation.

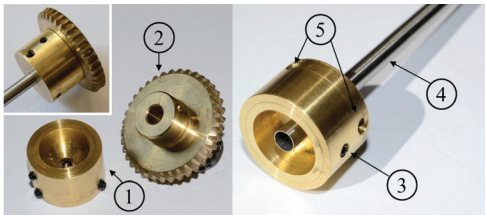


**Fig. 3 Detail views of the tube adapter (1). It is secured to the worm gear (2) with a set screw (3) to prevent rotation between them. The center hole is custom drilled to fit the specific tube it will hold (4). The tube is affixed to the tube adapter by three set screws (5) evenly distributed around its circumference.**

Translation of the carrier (and hence the tube it holds) is achieved by the rotation of the lead screw to which it is attached by a threaded lead screw nut (Fig. 2, part 8). Each carrier has two holes in it, one of which contains a nut for the lead screw that moves the carrier and the other of which allows the lead screw for the other carrier to pass freely through it. The nut is threaded into the main plate and secured with cyanoacrylate adhesive (Loctite 648) to prevent unthreading. Note that in an eventual clinical system, we would replace this nut with a press-fit nut to eliminate the use of adhesive, or choose a biocompatible and autoclavable adhesive such as Loctite 4014. The upper part of the carrier is secured to the guide block (Fig. 2, part 10) via the mounting plate (Fig. 2, part 9). Each guide block contains Frelon plane bearings to reduce friction. Two screws are countersunk into the bottom of the mounting plate and threaded into the lower portion of the main plate to secure the guide block to the upper assembly.

*2.1.2 Base*. The guide blocks allow the carriers to translate along a ceramic-coated aluminum rail (Fig. 1, part 3). The carriers are actuated individually with control knobs (Fig. 1, part 6) that rotate two steel lead screws (Fig. 1, part 2). Each control knob is attached to its lead screw via a small set screw. The lead screws are secured in place by the lead screw stops (Fig. 1, part 4), which are also set screwed to the lead screw. The lead screws are free on their other end to prevent binding as the carriers move along the track. The lead screws have a lead of 6.35 mm. Thus, one full turn of the control knob will translate the carrier approximately 6 mm. Polytetrafluoroethylene (PTFE) washers (Fig. 1, part 5) on either side of the back plate (Fig. 1, part 7) allow low friction rotation. A tube aperture block (depicted in Fig. 5) can be mounted to the front plate (Fig. 1, part 1). The aperture block, like the tube adapter, is a replaceable part with a hole drilled to match the diameter of the largest tube plus a small tolerance of approximately 0.25 mm. The front and back plates are each secured to the rail by two screws. Either plate can be removed for quick assembly or disassembly.

**2.2 Manual Deployment Procedure.** In order to deploy the cannula tip to a desired position, the inverse kinematic mapping from Cartesian space to joint space is required. This mapping will be described in Sec. 3. Once the mapping is known, the linear and angular positions of each tube can be determined. The operator of the device will then be provided with a step-by-step sequence of motions that he or she can implement using the control knobs on the actuation device.

## 3 Kinematic Mapping

While the actuation device is designed to be modular such that the design concept can be extended to cannulas composed of multiple tubes, here we consider a special case steerable cannula that can be deployed in a follow-the-leader method, such that the shaft of the cannula will follow the tip exactly during insertion [14]. This special case assumes that one outer straight tube is present, one middle curved tube is present, and an inner initially straight surgical device is inserted through the curved tube. Both the general model and the special case neglect friction. Hence, in the special case, there is no opportunity for torsion to arise provided that the curved tube is only allowed to axially rotate when it is fully inside the outer straight tube (so that tissue does not push on it in a torsional direction), which is something we require in our tube deployment sequence. One other assumption of the special case is that the overall stiffness of all tubes is high compared to the tissue through which they travel, such that the tissue will not deform the tubes (i.e., external loading can be neglected). The interested reader can find a more general kinematic model for a concentric tube robot that considers arbitrarily many tubes, arbitrary precurvatures (i.e., curves need not be circular) on each, and general external loading in Ref. [17].

**3.1 Kinematic Parameters.** The cannula is composed of two concentric tubes and a surgical tool inserted through the lumen (e.g., an ablator). The parameters describing the kinematic structure are depicted in Fig. 4(*a*). The outer tube is a straight stainless steel tube with length $L_1$, and the inner tube is made of superelastic Nitinol, has a length of $L_2$, and is curved into an arc of curvature $k_2$. The flexible but straight surgical tool with length $L_3$ is inserted through the inner lumen of the cannula. Since the outer tube and surgical tool are straight, only the inner tube's rotation about its axis by angle $\phi$ will affect the tip location. Hence, only rotation of the inner tube will be considered in the following. An example workspace for such a cannula is illustrated in Fig. 4(*b*).

The base frame is considered to be located at the center of the front plate aperture with the positive z-axis being tangent to the front plate pointing away from the device. The zero or home position of the concentric tubes is where all tips are at the front plate. When $\phi = 0$, positive curvature $(k_2 > 0)$ results in the backbone of the cannula tracing an arc in the y-z-plane with negative y-coordinates.

The kinematic structure of this steerable cannula can be described by considering that there are three main links or segments: (1) the first link with length $\ell_1$ where all tubes are combined, (2) the second link with length $\ell_2$ where the curved part of the inner tube and surgical tool are combined, and (3) the third and final straight link with length $\ell_3$ where the surgical tool extends the tip of the inner tube. These link lengths are combinations of the total lengths of each tube ($L_1$, $L_2$, and $L_3$), and the translational distances between the distal ends of the tubes and the base frame ($D_1$, $D_2$, and $D_3$). They can be calculated as follows:

$$\ell_1 = L_1 - D_1 \tag{1}$$

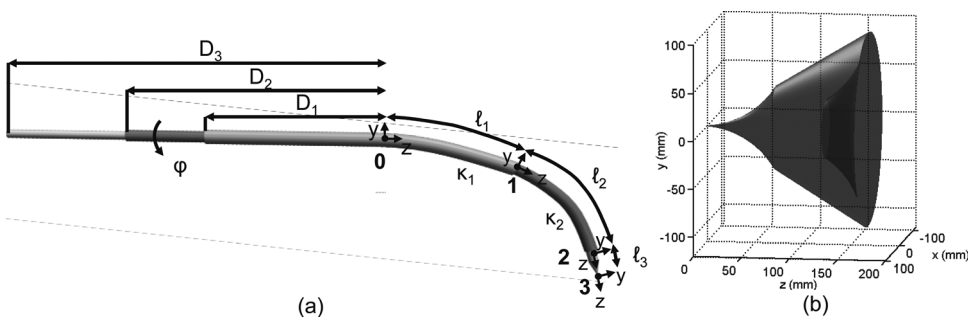


**Fig. 4 Kinematics and workspace of a steerable cannula. (*a*) Parameter definitions for the kinematic mapping. Note that only the tube whose base position if specified by $D_2$ is precurved into a circular shape. The outer tube and inner surgical instrument are elastic but initially straight. In sections $\ell_1$ and $\ell_2$, the middle tube deforms the others. (*b*) An example workspace for a cannula with $L_1 = 128.1$ mm, $L_2 = 214.1$ mm, $k_1 = 0.037$ mm$^{-1}$, and $k_2 = 0.0108$ mm$^{-1}$.**

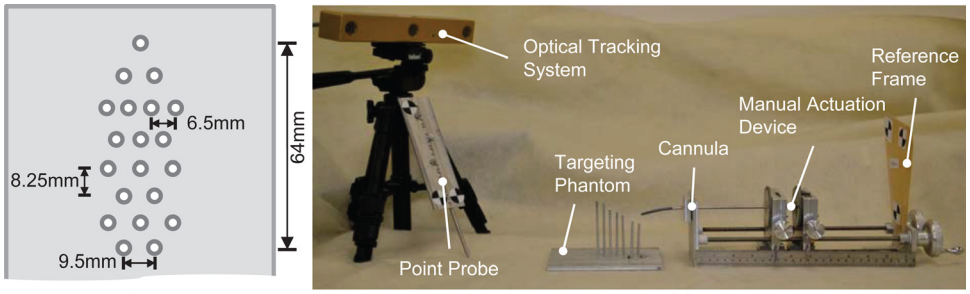


**Fig. 5 Experimental assessment of the manual actuation device's accuracy. (*a*) Dimensions of the targeting phantom used in free space and ultrasound-guided targeting experiments in ethanol solution. (*b*) Experimental setup for freespace experiments.**

$$\ell_2 = L_2 - D_2 - \ell_1 \tag{2}$$

$$\ell_3 = L_3 - D_3 - \ell_2 - \ell_1 \tag{3}$$

The curvature of the first and second link can be determined as the resultant curvature of the overlapping tubes and surgical instrument as

$$\kappa_1 = \frac{E_2 I_2 k_2}{E_1 I_1 + E_2 I_2 + E_3 I_3} \tag{4}$$

$$\kappa_2 = \frac{E_2 I_2 k_2}{E_2 I_2 + E_3 I_3} \tag{5}$$

where $E_i$ is the Young's Modulus, $I_i$ is the cross sectional moment of inertia, and $k_i$ is the curvature. $\kappa_1$ will be much less than $\kappa_2$ because the outer tube is straight and much stiffer than the curved inner tube.

**3.2 Forward Kinematics.** The forward kinematics [8] maps the tip position of the cannula to a given set of actuation inputs $(D_1, D_2, \phi, D_3)$. The main three links described above provide the mapping from the base frame 0 to the tip frame 3. The homogeneous transformation matrices describing the mapping between two succeeding frames are

$${}^0\mathrm{T}_1 = \begin{bmatrix} \cos\phi & -\sin\phi\cos\theta_1 & \sin\phi\sin\theta_1 & (-\sin\phi/\kappa_1)(\cos\theta_1 - 1) \\ \sin\phi & \cos\phi\cos\theta_1 & -\cos\phi\sin\theta_1 & (\cos\phi/\kappa_1)(\cos\theta_1 - 1) \\ 0 & \sin\theta_1 & \cos\theta_1 & \sin\theta_1/\kappa_1 \\ 0 & 0 & 0 & 1 \end{bmatrix}$$

$${}^1\mathrm{T}_2 = \begin{bmatrix} 1 & 0 & 0 & 0 \\ 0 & \cos\theta_2 & -\sin\theta_2 & (\cos\theta_2 - 1)/\kappa_2 \\ 0 & \sin\theta_2 & \cos\theta_2 & \sin\theta_2/\kappa_2 \\ 0 & 0 & 0 & 1 \end{bmatrix}$$

$${}^2\mathrm{T}_3 = \begin{bmatrix} 1 & 0 & 0 & 0 \\ 0 & 1 & 0 & 0 \\ 0 & 0 & 1 & \ell_3 \\ 0 & 0 & 0 & 1 \end{bmatrix}$$

where $\theta_1 = \kappa_1 \ell_1$ and $\theta_2 = \kappa_2 \ell_2$. Hence, the forward kinematic mapping is given by

$${}^0\mathrm{T}_3 = {}^0\mathrm{T}_1 \, {}^1\mathrm{T}_2 \, {}^2\mathrm{T}_3 \tag{6}$$

**3.3 Inverse Kinematics.** The inverse kinematic mapping relates a desired Cartesian tip position $(x, y, z)$ to a set of actuation inputs $(D_1, D_2, \phi, D_3)$. Hence, the translational part of ${}^0\mathrm{T}_3$ (first three elements of the right most column) must equal the desired position, which is a system of nonlinear equations described in terms of the actuation inputs. We solve this numerically using MATLAB's fminsearch function with the objective to minimize the Cartesian position error. This unconstrained optimization requires a good initial guess in order to converge. We, therefore, create a lookup-table of Cartesian tip positions by sampling the workspace using a uniform discretization of actuation inputs. For each sample, we calculate the tip error with respect to the desired target position. The minimum error value in this lookup table gives a good initial guess for $(D_1, D_2, \phi, D_3)$.

## 4 Accuracy Assessment

In order to assess the accuracy achievable with the manual actuation device, we performed targeting experiments in free space and in a more clinically representative setting using image-guidance with a tracked 2D ultrasound system. In all cases, an optical tracking system was utilized for measuring desired positions with respect to a reference frame represented by a rigid body (Fig. 5(*b*), right). The tube parameters were $L_1 = 128.1$mm, $L_2 = 214.1$ mm, $k_1 = 0.0034$ mm$^{-1}$, and $k_2 = 0.0113$ mm$^{-1}$. The outer stainless steel tube had an outside diameter of 4.20 mm and an inside diameter of 3.68 mm. The curved Nitinol tube had an outside diameter of 3.55 mm and an inside diameter of 2.80 mm. We note that these tube diameters should, in general, be selected to accommodate the specific interventional device the user of the system wishes to deploy and are essentially arbitrary from the perspective of the actuation mechanism and system presented in this paper. While it is preferable to use smaller diameter tubes to reduce tissue disruption during insertion, the relatively large tubes used in our study were an artifact of prior research in deploying a 2.4 mm diameter acoustic ablator into liver tumors (see Ref. [14]). Research to miniaturize that particular acoustic ablator is ongoing. In the accuracy assessments that follow, we used a simulated ablator consisting of a small, conic thermoplastic tip, making $\ell_3$ fixed at 6.06 mm.

**4.1 Registration and Calibration.** To deploy the cannula to a desired target position given in the reference frame, the position has to be transformed into the cannula coordinate system. Hence, a registration step has to be performed prior to targeting experiments, i.e., determination of the transformation from the reference frame to the local cannula frame.

This transformation can be determined using point-based registration [18]. This requires acquisition of two corresponding point sets in the respective coordinate frames. In our case, these are cannula tip positions in the coordinate frame given by the kinematic model and the corresponding physical cannula tip positions

**Table 1 Actuation inputs ($D_1, D_2, \phi$) for registration poses**

| $D_1$ (in mm) | $D_2$ (in mm) | $\phi$ (in deg) |
|---|---|---|
| 0 | 0 | 0 |
| 10 | 35 | 0, 45, 90, 180, 235, 270 |
| 15 | 50 | 0, 45, 90, 180, 235, 270 |
| 25 | 70 | 0, 45, 90, 180, 235, 270 |
| 40 | 85 | 0, 45, 90, 180, 235, 270 |

measured with respect to reference frame with an optically tracked point probe. The 25 cannula poses in Table 1 were used for registration.

The measurement of the curvature parameters $\kappa_1$ and $\kappa_2$ contains some uncertainty. In order to optimize the accuracy of the kinematics, we combine the registration step with a calibration step. This means that the two curvature parameters are fit along with the frame parameters in the point-based registration process. This was implemented using MATLAB's fminsearch function.

**4.2 Targeting Phantom.** To allow for direct comparison of these results, we constructed a targeting phantom. The phantom is made of an aluminum plate with a thickness of 6.9 mm. A total of 20 holes were drilled through the plate following the pattern depicted in Fig. 5(*a*). Six aluminum dowels serve as target locations and can be placed as desired in the drilled holes. The dowels have varying lengths of 51.3 mm, 57.7 mm, 62.5 mm, 68.7 mm, 73.7 mm, and 79.9 mm.

**4.3 Free Space Experiments.** For the free space experiments, we used an optical tracking system (Micron Tracker H3-60, RMS 0.2 mm, ClaronTechnology) and affixed a reference rigid body to the back plate of the actuation device (see Fig. 5(*b*)). The tip of a tracked point probe was localized with respect to the reference frame. Experiments were performed on the benchtop, with the manual actuation device and the targeting phantom fixed in place.

A total of 84 target points were each measured three times using a tracked point probe. To reduce measurement noise for each target point, the average of the three measurements was used. Each target point was then transformed into the cannula frame using the registration information. Using the inverse kinematics, a set of actuation inputs was determined for each target point. The cannula was then deployed to these actuation inputs and the resulting tip position measured with the tracked point probe. To reduce measurement noise and manual deployment error, the deployment of the cannula to the desired target position was performed three times and the tip position averaged. Each tip position was finally transformed into the cannula frame using the registration information. The experimental setup for the free space experiments is shown in Fig. 5(*b*). The achieved tip positions were compared to the desired cannula tip positions as shown in Table 2.

**4.4 Image-Guided Targeting Experiments.** Targeting experiments were also performed in an image-guided setting using ultrasound as the imaging modality. Here, a tracked 2D ultrasound system (ACUSON, Siemens Medical Solutions Inc.) with a linear transducer (VFX-9, Siemens Medical Solutions Inc.) and an optical tracking system (Hybrid Polaris Spectra, RMSE 0.35 mm, Northern Digital Inc., Canada) was used. A rigid body was affixed close to the fixed manual actuation device and served as the reference frame. Another rigid body was attached to the ultrasound transducer for tracking with respect to the reference frame. The calibration error of the tracked 2D ultrasound system was 1.0±0.5mm (see Ref. [15] for the calibration methodology). For detailed information on ultrasound calibration, the reader is referred to the review paper on the subject by Mercier et al. [19]. We also note that standard surgical needles can cause imaging artifacts in ultrasound, which propagate away from the transducer, starting at the needle. Our steerable cannula can create the same kind of imaging artifact. To ensure that these artifacts would not interfere with targeting, we selected insertion directions for the cannula that would not interpose it between the ultrasound probe and the desired target. Such directions of insertion are typically available clinically and are used in standard US-guided needle insertion procedures.

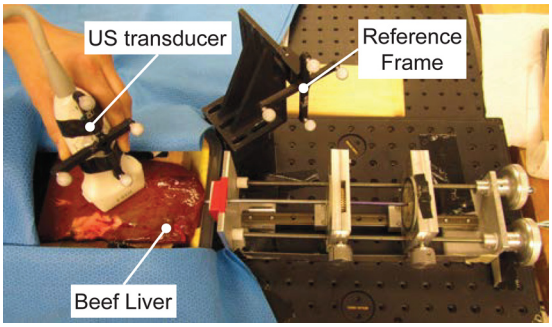


**Fig. 6 Experimental setup for image-guided targeting experiment in *ex vivo* beef liver using tracked 2D ultrasound**

*4.4.1 Ethanol-Water Solution.* In the first set of targeting experiments, the targeting phantom was placed into a container with a $C_2H_6O$ (9.5%) solution. The same ethanol solution was also used for calibrating the ultrasound probe since its speed-of-sound is close to that of liver (1540 m/s). The cannula entered the container through a hole in a rubber tapered plug on the side of the container.

A total of 55 targets were imaged using the tracked ultrasound transducer. Each target was manually selected in each ultrasound image. Deployment parameters were determined as described in Sec. 4.3. The cannula tip position was then imaged using the tracked ultrasound probe for each target and manually selected in each ultrasound image. The targeting error was determined as described in Sec. 4.3.

*4.4.2 Ex Vivo Liver.* In a second set of targeting experiments, a fresh piece of *ex vivo* bovine liver was used. The liver was placed in a Styrofoam container and was accessible to the cannula through a hole in the side of the container. The Styrofoam container was fixed to the bench. In order to produce well-defined and identifiable targets inside the liver, thin wooden dowels were inserted that appear as circular targets in the ultrasound image. Target locations were randomly picked and spread over the liver. Figure 6 shows the experimental setup. A total of ten targets were imaged using the tracked ultrasound transducer. The experimental protocol and error calculations were the same as those described previously for the ethanol-water solution.

## 5 Results

The registration and calibration described in Sec. 4.1 was performed five times. The average registration error without performing the calibration step was 2.66 mm, whereas the average registration error including calibration was 1.31 mm. The registration used for the targeting experiments had an error of 1.18 mm with calibrated curvature values of $\kappa_1 = 3.4$ mm$^{-1}$ and $\kappa_2 = 11.3$ m$^{-1}$. The results of the freespace and image-guided targeting experiments are summarized in Table 2. The mean error was approximately 3.3 mm across all experiments.

**Table 2 Mean error ($\overline{\Delta}$) and standard deviation (SD) in x-, y-, and z-directions and Euclidean norm for freespace, ultrasound-guided $C_2H_6O$ (9.5%), and bovine liver targeting experiments. All values in mm.**

| | | x | y | z | $\|.\|_2$ |
|---|---|---|---|---|---|
| Free space | $\overline{\Delta}$ | 2.20 | 1.91 | 0.66 | 3.34 |
| | SD | 1.32 | 1.59 | 0.60 | 1.56 |
| $C_2H_6O$ (9.5%) | $\overline{\Delta}$ | 1.87 | 1.93 | 1.06 | 3.31 |
| | SD | 1.32 | 1.97 | 0.54 | 1.80 |
| Liver | $\overline{\Delta}$ | 2.96 | 0.92 | 0.48 | 3.32 |
| | SD | 2.79 | 0.67 | 0.43 | 2.66 |

## 6 Discussion

The manual actuation device described in this paper meets our design objectives. The entire assembled device is small; it fits within an envelope of 100 mm × 90 mm × 260 mm. Including tubes, the device weighs less than 2 kg. The design is straightforward and inexpensive to manufacture. Most importantly, the design allows sterilization in an autoclave, facilitating future use in clinical studies.

The accuracy achievable with the manual actuation device depends on the mechanical parts and assembly tolerances, the user error in manual operation of the device, and also the optical tracking and registration errors. The device is subject to some backlash in the gears that reduces the overall accuracy and repeatability of the device. Furthermore, the manual adjustment of the control knobs to the desired actuation inputs is subject to human error, in addition to limits imposed by the resolution of linear and angular scales. However, despite these sources of error, our experiments resulted in an overall targeting error of 3.3 mm, which is considered to be sufficient for thermal tumor ablation in the liver and potentially other soft tissue targeting applications. The accuracy achieved with the manual actuation device is comparable to the results obtained with a robotically controlled actuation device in a similar set of experiments [15].

One may wonder what effect introducing a new ablator with variable stiffness along its length may have on our device and whether accurate targeting can still be achieved. We note that the effect of such an ablator on the overall curve of the device is fully described by our prior beam mechanics models [17]. In this case, we would recommend a modified deployment sequence where the ablator is not present during targeting, and is inserted after the tip of the inner tube reaches the desired point in tissue. The insertion of the ablator at this time would deform the cannula, which would in turn deform the tissue media. In this case, we hypothesize that the net effect would be that the target point in tissue would move with the cannula tip, and the ablator would still arrive there.

We also note that in the future it may be necessary to compensate for tissue deformation during insertion of a cannula with our device. It is known that tissue deformation can move a target away from a needle as it is inserted, even with standard straight surgical needles. Our system will also be subject to these effects. Thus, in the future, depending on the targeting accuracy required, it may be useful to add an ultrasound-based visual servoing element to our system. If this were to be done, it would likely be useful to motorize the device (as was done in Ref. [15]) to relieve the surgeon of the burden of executing many manual motions on the control knobs in real time as the cannula advances.

## 7 Conclusions and Future Work

In this paper, we have presented the design of a manual actuation device for concentric tube steerable cannulas that is versatile, compact, and accurate. The device is designed to be operated in a straightforward manner so that learning curves are not expected to present a barrier to its implementation in surgical settings. The fully assembled unit is also autoclavable, making it suitable for clinical implementation. We note that the device will have to be anodized before in-patient use, stainless steel components will have to be passivated, and the brass components need to be replaced by Ultem or PEEK to assure biocompatibility.

While the achieved accuracy is sufficient for some medical applications in soft-tissue, we anticipate that the targeting error can be reduced by using a more accurate localization system, improving the calibration and registration accuracy, and improving the tolerances in the gear train in the tube carrier mechanism. We intend to conduct human trials to validate the effectiveness of the device in a clinical setting.

To conclude, we have presented a manual device for deployment of steerable cannulas. We believe that this device will be useful for medical applications that do not require a large number of concentric tubes or tubes that must be dynamically manipulated. Thus, we believe it can be a first step toward acceptance in the medical community for future robotic versions of the device, and it will facilitate initial human studies by streamlining the IRB and FDA approval processes.

## Acknowledgment

This work was funded in part by Award No. IIS-1054331 from the National Science Foundation and Award No. R44 CA134169 from the National Institutes of Health. The content is solely the responsibility of the authors and does not necessarily represent the official views of the National Science Foundation or the National Institutes of Health.

The authors thank Thomas Pheiffer, Janet Ondrake, Amber Simpson, and Michael Miga from the Department of Biomedical Engineering at Vanderbilt University for providing the ultrasound system and support during the experiments involving image-guidance. We also want to thank our project partners Emad Boctor from Johns Hopkins University and Chris Diederich from University of California for motivating this research.

## References

[1] DiMaio, S., and Salcudean, S., 2003, "Needle Insertion Modeling and Simulation," IEEE Trans. Rob. Autom., **19**(5), pp. 864–875.
[2] Okazawa, S., Ebrahimi, R., Chuang, J., Salcudean, S., and Rohling, R., 2005, "Hand-Held Steerable Needle Device," IEEE/ASME Trans. Mechatron., **10**(3), pp. 285–296.
[3] Webster, R. J., III, Kim, J. S., Cowan, N. J., Chirikjian, G. S., and Okamura, A. M., 2006, "Nonholonomic Modeling of Needle Steering," Int. J. Robot. Res., **25**(5-6), pp. 509–525.
[4] Glozman, D., and Shoham, M., 2007, "Image-Guided Robotic Flexible Needle Steering," IEEE Trans. Rob., **23**(3), pp. 459–467.
[5] Kallem, V., and Cowan, N. J., 2009, "Image Guidance of Flexible Tip-Steerable Needles." IEEE Trans. Rob., **25**(1), pp. 191–196.
[6] Misra, S., Reed, K. B., Schafer, B. W., Ramesh, K. T., and Okamura, A. M., 2010, "Mechanics of Flexible Needles Robotically Steered Through Soft Tissue," Int. J. Robot. Res., **29**(13), pp. 1640–1660.
[7] Webster, R. J., III, Okamura, A. M., and Cowan, N. J., 2006, "Toward Active Cannulas: Miniature Snake-Like Surgical Robots," Proceedings of the IEEE/RSJ International Conference on Intelligent Robots and Systems (IROS 2006), Beijing, China, October 9–15, pp. 2857–2863.
[8] Webster, R. J., III, Romano, J. M., and Cowan, N. J., 2009, "Mechanics of Precurved-Tube Continuum Robots," IEEE Trans. Rob., **25**(1), pp. 67–78.
[9] Dupont, P. E., Lock, J., Itkowitz, B., and Butler, E., 2010, "Design and Control of Concentric-Tube Robots," IEEE Trans. Rob., **26**(2), pp. 209–225.
[10] Burgner, J., Swaney, P. J., Rucker, D. C., Gilbert, H. B., Nill, S. T., Russell, P. T., Weaver, K. D., and Webster, R. J., 2011, "A Bimanual Teleoperated System for Endonasal Skull Base Surgery," Proceedings of the IEEE/RSJ International Conference on Intelligent Robots and Systems (IROS 2011), San Francisco, September 25–30, pp. 2517–2523.
[11] Gosline, A. H., Vasilyev, N. V., Butler, E. J., Folk, C., Cohen, A., Chen, R., Lang, N., del Nido, P. J., and Dupont, P. E., 2012, "Percutaneous Intracardiac Beating-Heart Surgery Using Metal MEMS Tissue Approximation Tools," Int. J. Robot. Res., **31**(9), pp. 1081–1093.
[12] Rucker, D. C., Webster, R. J., III, Chirikjian, G. S., and Cowan, N. J., 2010, "Equilibrium Conformations of Concentric-Tube Continuum Robots," Int. J. Robot. Res., **29**(10), pp. 1263–1280.
[13] Boctor, E. M., Stolka, P., Kang, H.-J., Clarke, C., Rucker, C., Croom, J., Burdette, E. C., and Webster, R. J., III, 2010, "Precisely Shaped Acoustic Ablation of Tumors Utilizing Steerable Needle and 3D Ultrasound Image Guidance," SPIE Med. Imaging, **7625**, p. 76252N.

[14] Burdette, E. C., Rucker, D. C., Prakash, P., Diederich, C. J., Croom, J. M., Clarke, C., Stolka, P., Juang, T., Boctor, E. M., and Webster, R. J., III, 2010, "The ACUSITT Ultrasonic Ablator: The First Steerable Needle With an Integrated Interventional Tool," SPIE Med. Imaging, **7629**, p. 76290V.
[15] Swaney, P. J., Burgner, J., Pheiffer, T. S., Rucker, D. C., Gilbert, H. B., Ondrake, J. E., Simpson, A. L., Burdette, E. C., Miga, M. I., and Webster, R. J., III, 2011, "Tracked 3D Ultrasound Targeting With an Active Cannula," SPIE Med. Imaging, **8316**, p. 83160R.
[16] Bruns, T., Tucker, J., Rucker, D. C., Swaney, P. J., Boctor, E., Burdette, E. C., Burgner, J., and Webster, R. J., III, 2011, "Design of an Autoclavable Active Cannula Deployment Device," ASME J. Med. Devices, **5**(2), p. 027538.
[17] Rucker, D. C., Jones, B. A., and Webster, R. J., III, 2010, "A Geometrically Exact Model for Externally Loaded Concentric-Tube Continuum Robots," IEEE Trans. Rob., **26**(5), pp. 769–780.
[18] Fitzpatrick, J. M., 2010, "The Role of Registration in Accurate Surgical Guidance," Proc. Inst. Mech. Eng., Part H: J. Eng. Med., **224**(5), pp. 607–622.
[19] Mercier, L., Langø, T., Lindseth, F., and Collins, D. L., 2005, "A Review of Calibration Techniques for Freehand 3-D Ultrasound Systems," Ultrasound Med. Biol., **31**(4), pp. 449–471.